MANUFACTURING OPTIONS FOR SECONDARY AIRCRAFT CFRP SANDWICH COMPONENTS

Duncan A. Crump*, Janice M. Dulieu-Barton*, John Savage**
***University of Southampton, ****Smiths Aerospace**

Keywords: *Aircraft, CFRP, Sandwich, Structure.*

Abstract

The objective of this research is to reduce the cost of carbon fibre sandwich component manufacture for use in aircraft secondary structure. The current paper describes the design of generic components to be representative of secondary structure components and the design of a full-scale pressure load test rig to provide validation for structural analysis being carried out using Finite Element analysis (FEA). For comparison to the FEA model, optical techniques will be used to measure stress/strain during the mechanical tests. The current paper has described the results of a feasibility study of three such optical techniques; namely Thermoelastic Stress Analysis (TSA), Pulse Phase Thermography (PPT) and Digital Image Correlation (DIC). These feasibility tests showed TSA and DIC can offer useable results for measurements of carbon fibre sandwich structure.

1 Introduction

Composite sandwich structure components are known to offer a weight saving over traditional metallic parts. The current trend is for lighter aircraft that are more fuel efficient to reduce fuel cost and reach environmental targets. The objective of this research is to reduce the cost of carbon fibre sandwich component manufacture for use in aircraft secondary structure.

The cost of manufacturing composite components is high due to the complexity of the process. Traditionally, aerospace standard secondary structures are produced by hand lay-up of prepreg materials that are cured in an autoclave. This process is labour intensive, uses expensive materials and the autoclave requires high capital and running costs. Therefore a number of approaches to reduce the costs of the manufacture of these components have been suggested [1].

The goal of the investigation is to consider the mechanical performance of components produced by a reduced cost manufacturing process that uses less expensive materials. The components are cured using the Resin Film Infusion (RFI) technique that involves the use of layers of dry fabric and resin film laid up on a tool. The applied vacuum draws the resin through the thickness of the fibre stack, a much shorter path than that required for standard resin infusion [2]. The overall objective is to compare the performance of the full-scale components, representative of secondary structure, manufactured by traditional methods to components manufactured using the RFI approach. The aim is to carry out structural analysis using finite element analysis (FEA) with a full experimental validation using optical techniques.

The present paper describes the representative components of secondary structure components that are considered and the materials and manufacturing processes available to create such parts. A detailed description of the design of a mechanical testing rig that is capable of subjecting the panels to realistic service loads is provided. Finally, the feasibility of three different methods for full-field optical assessment is investigated.

2 Manufacturing Options

A manufacturing option is defined by the materials and manufacturing processes that are utilised to produce the component. Five manufacturing options are investigated in this research, and are listed below:

1. Uni-directional prepreg tape cured in an autoclave.
2. Five-harness satin weave prepreg (8552S/37%/AGP280 from Hexcel) cured in an autoclave.
3. Non-crimped fabric (NC2) and resin film cured in an autoclave.

4. Five-harness satin weave fabric (AGP280) and resin film using RFI process.
5. Non-crimped fabric (NC2) and resin film using RFI process.

Manufacturing option 1 (MO1) is the traditional approach that requires the largest labour effort to produce the component from numerous thin plies. Option 2 (MO2) is regarded as the current ideal solution that provides adequate performance and quality for the aerospace industry while using the thicker woven material reduces some of the labour content. Option 3 (MO3) uses the new RFI process and resin film with the fabric used in option 2. Option 4 (MO4) investigates the performance of the novel material cured using the traditional process. Finally option 5 (MO5) represents the novel manufacturing option in which both the material and process has been altered.

3 Tensile Test Results

An initial comparison of the manufacturing options can be made through mechanical characterisation of tensile specimens. Using specimens of dimensions shown in Figure 1 and test methods from ASTM D3039, material manufactured from MO 2 and MO 5 has been characterised for strength and stiffness in a tensile test. The data obtained from these tests will also be of use to input into an FEA model. The specimens were subjected to a quasi static tensile load at 2 mm/min (as per ASTM) using an Instron servo-hydraulic test machine. Measurements of load, extension and strain were taken to provide the properties given in Table 1. For each property six readings were taken from six different specimens.

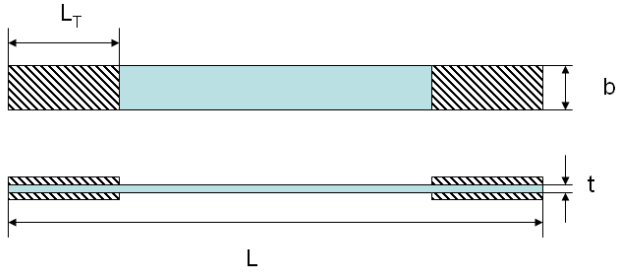

Fig 1. Tensile specimen dimensions

Where L = 250 mm, L_T = 55 mm, b = 15 mm and t = 3 mm.

MO 2 uses a five harness woven fabric, while MO5 uses a non-crimp woven fabric. Both have equal fibre weight in the longitudinal and transverse directions. This is attested to by the relative equality of the strength and stiffness results in the longitudinal and transverse directions. The results show a trend that while the material manufactured by RFI is less stiff than that manufactured in the autoclave, it has a higher strength value. Both sets of specimens have similar fibre volume fractions (V_f). The autoclaved cured prepreg has a V_f of 53.3% while the RFI material has a V_f of 52.6%. Therefore differences in the mechanical properties must be a consequence of differences in the materials and not the manufacturing process.

Table 1. Mechanical properties of material

Property	MO2 - Prepreg	MO5 - Infusion
0° Strength (MPa)	753.9	1005
90° Strength (MPa)	739.3	-
0° Stiffness (GPa)	64.82	61.1
90° Stiffness (GPa)	66.65	58.6
μxy	0.0153	-

4 Design of Full-Scale Tests

The objective of the current research is to compare the performance of secondary structure manufactured from the five different manufacturing options. For the purposes of this work the comparison will be made using full-scale mechanical tests on representative generic panels that can be used to validate an FE model developed for future analysis.

4.1 Generic Panel

This study is considering secondary structure on aircraft wings, in particular trailing edge access panels on commercial passenger aircraft (see Figure 2). Such panels are bolted to the main wing beam and 'A-frames' along three sides, allowing one of the longer edges to be free to deflect under the service loads. The panels are subjected to aerodynamic out-of-plane pressure loads across the flat surface and must withstand the in-plane stress induced through the bolts from the wing bending strain as the wing beam deflects during service.

For the purposes of this work the loading configuration is simplified to a pressure load over the surface. To make a comparison of the performance of the components made from the manufacturing options it was decided to design a full-scale generic component that are representative

of current industry secondary structure wing trailing edge components.

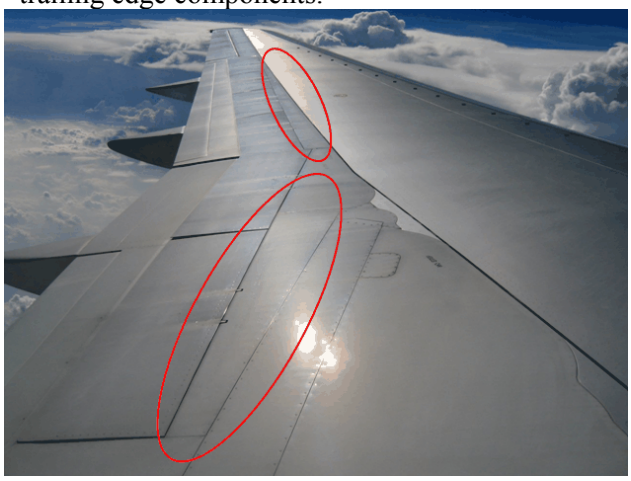

Fig 2.Secondary structure on passenger aircraft

A review of previous designs of secondary structure that have been manufactured at Smiths Aerospace from CFRP sandwich has identified a number of 'common' features:

- Quasi-isotropic lay-up, 24 plies @ 0.125mm per ply,
- Panels are long and narrow – between 700 and 1500 mm long while 300 mm wide,
- Cut-outs and notches are common to account for position of panel,
- Details such as inserts and solid carbon pucks for attachments,
- Core geometry generally simplistic.

Consideration of the above features allowed the development of the geometry of three 'generic panels' (see Figure 3 (a-c)). It has been decided that features such as inclusions and attachments are beyond the scope of this research and would lead to stress concentration problems that make evaluation too complex at this stage. The generic panels are flat and have a plan area of 0.9 m x 0.3 m. The honeycomb core is one inch thick and a non-core stiffened flange is included as this is a key feature in such panels. The flange has a cured thickness of 3 mm.

The first generic component design (see Figure 3(a)) has a simple rectangular core-stiffened section and represents the most basic case. Generic panel two (Figure 3(b)) incorporates a cut-out that may be required to accommodate a protrusion from an adjacent panel. The cut-out necessitates a recess in the core stiffener that is accomplished by two separate cores. Finally generic panel three (Figure 3(c)) incorporates a more complex core stiffener shaped to accommodate the cut-out.

Considering the baseline of a panel laminated from twenty four unidirectional plies, a lay-up was developed that would offer a quasi-isotropic panel and would take into account known design rules to minimise stress coupling and maximise the strength properties. It was also crucial to define a lay-up that could be achieved when the material was more complex, such as the four-layered NC2 material (consisting of 0°, 45°, -45°, 90°). The following laminate was decided upon:

$$[0°, 45°, -45°, 90°, 90°, -45°, 45°, 0°, 0°, 45°, -45°, 90°]_S$$

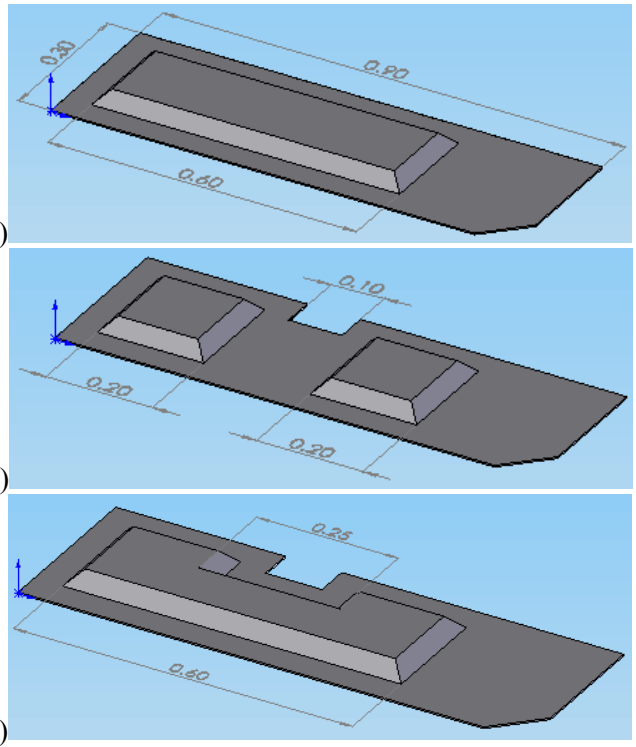

Fig 3 . (a) Generic Panel 1, (b) Generic Panel 2, (c) Generic Panel 3

4.2 Finite Element (F.E.)

Through discussions with engineers at Smiths Aerospace it was decided that the generic panels must withstand a pressure load of 27.58 kN/m^2 to model in-service conditions. For the purposes of this study, it was important that such a load would provide sufficient stress/deformation in the panels to allow measurement and a 'reasonable' investigation of the performance of such panels manufactured through the five MOs. To gain an

insight into the behaviour of such a panel under the service load, an FE model was constructed using ANSYS 8.1.

The model was constructed using two basic shapes. The first is the size and shape of the total plan area of the generic panel. The second, the size and shape of the honeycomb core, is extruded to form the volume of the core by a z-axis offset with taper in x and y to produce the chamfered core shape. The first area and those areas that bound the core volume are the carbon fibre skins. It has been assumed that the honeycomb is a singular isotropic, solid volume with the relevant associated properties. The flange area contains all twenty four plies, while the areas bounding the volume have sections of twelve plies thereby summing to twenty four. Using Solid185, an eight noded brick element for the core and Shell181, a four noded element suitable for laminates, for the carbon fibre skins the model has been meshed (see Figure 4). To represent the service constraints the model is held on three sides, the two short sides and one of the longer sides, such that zero deflection in all axes is allowed. The global coordinates are in Figure 4. To maintain the fibre orientation on the chamfered edges of the core stiffener it was necessary to alter the individual element coordinate systems such that z remained perpendicular to the surface.

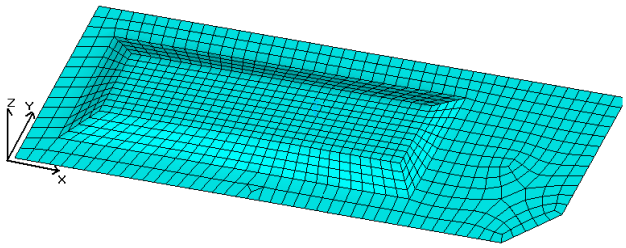

Fig 4. FE mesh for generic panel

Table 2. Material properties for FE model

Property	Value
E_x (GPa)	137
E_y (GPa)	9
E_z (GPa)	9
ν_{xy}	0.3
ν_{yz}	0.02
ν_{xz}	0.02
G_{xy} (GPa)	7.1
G_{yz} (GPa)	7.1
G_{xz} (GPa)	7.1

The model used material data from MO1, uni-directional prepreg tape (see Table 2), cured in an autoclave, because this was perceived as the stiffest and strongest material therefore defining the maximum load required for the experiments. The generic panel is a relatively thin structure under a pressure load that would induce relatively large deflections. For this reason the model was solved using a geometrically non-linear solver. Initial results from the model indicated a maximum deflection of the order of 10 mm

4.3 Mechanical Testing Rig

The FE proved the service load condition offered measurable deflections. Therefore, it was possible to design a rig to validate the FE model of the generic panel. It was important to produce a rig capable of imitating the pressure load condition the panels are subjected to in-service while ensuring stress concentrations were kept to a minimum. To make a comparison with an FE model, full-field measurement of stress/deformations was contemplated. At the University of Southampton there is equipment available to undertake a number of optical full-field analysis techniques. Visual techniques require 'line-of-sight' to the component, therefore the rig must be designed to keep the top surface free from obstructions. The load is to be applied by an Instron servo-hydraulic test machine through a loading frame that pulls the panel against a water filled cushion to apply a pressure load on to the surface of the panel. It was decided that a water filled cushion would provide a consistent loading due to the incompressible nature of water.

The rig has been designed in two parts, a table structure that will support the water cushion ensuring the correct reaction force is transferred into the test panel, and a loading rig that is bolted to the perimeter of the test panel and clamped in the jaws of the test machine's loading ram to pull the panel against the pressurised cushion. It was important that once constructed this rig would be able to withstand the loads required for the test, while providing the required deflection. To this end an FE model was formed of the two separate sections of the rig. The analysis was performed at 100 kN, the maximum load available from the Instron machine. During testing, the rig will not have to withstand such high loads, but this provides an adequate safety factor and will account for significant overload. Figures 5 and 6 show a plot of the stress distribution in the table structure and loading rig respectively.

From this first iteration a number of stress concentrations were discovered and the design was modified to provide extra strength in the required areas. The final design can be seen in Figure 7.

The dark panel at the top of Figure 7 is the test panel, and the lighter grey structure forms the pressure rig. The pressure rig is currently under construction and it is planned to commence full-scale tests in July 2007. To assess the feasibility of using optical techniques with this rig some bending tests on sandwich structure have been carried out and are described in the next section.

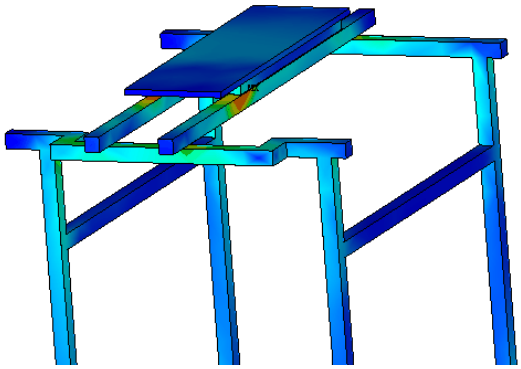

Fig 5. Stress distribution in the table structures

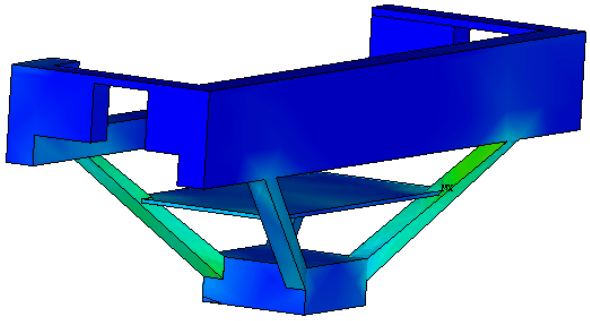

Fig 6. Stress distribution in the loading rig

5 Full-Field Monitoring Techniques

The mechanical rig has been designed such that optical accessibility to the surface of the panel is possible to allow full-field analysis of the stress/deformation. To investigate if these techniques can produce data that can be interpreted in terms of damage and stress some initial tests have been conducted. The tests involved the use of single skin material, similar to that used in the generic panels and carbon fibre sandwich structure. The sandwich panels were subjected to bending as will be experienced by the service panels (see Figure 8). To investigate the feasibility of optical techniques three techniques, namely thermoelastic stress analysis (TSA), pulse phase thermography and digital image correlation (DIC) are used.

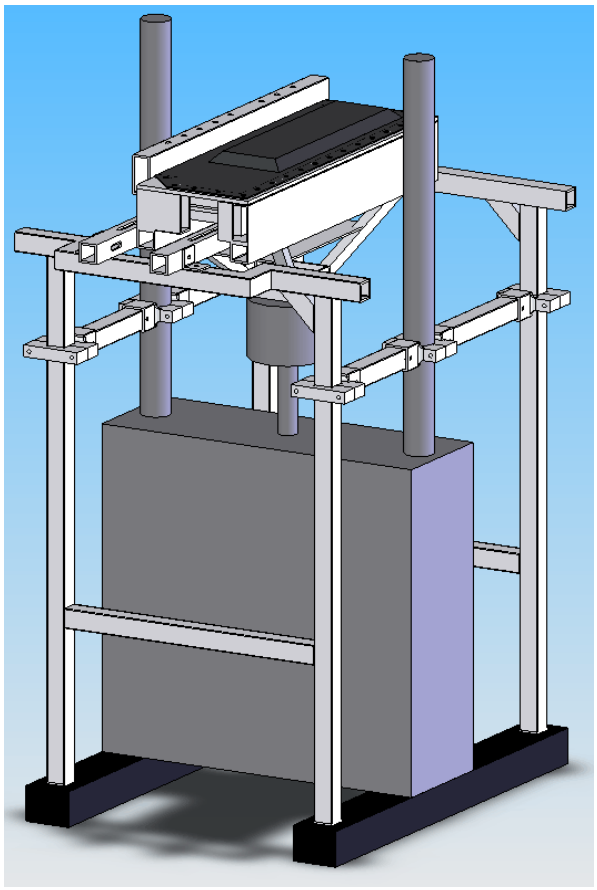

Fig 7. Final pressure rig design

(a)

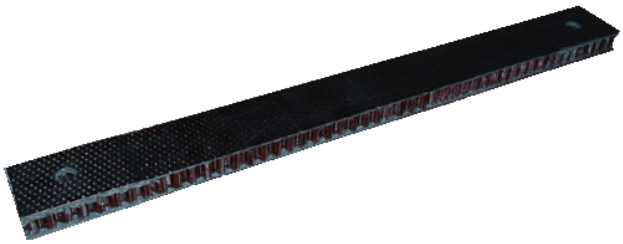

(b)

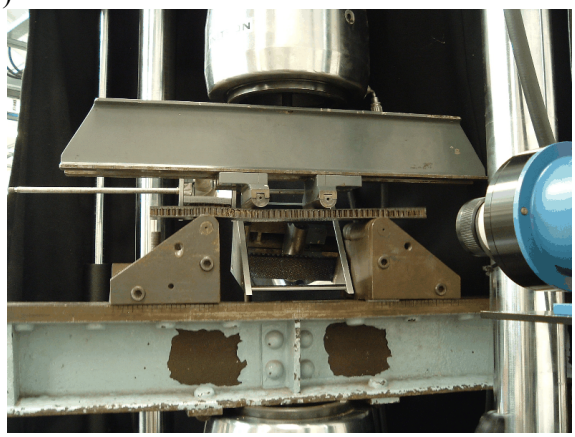

Fig 8. (a) Sandwich beam specimen, (b) beam under loading

5.1 Thermoelastic Stress Analysis (TSA)

TSA is a well-established, non-contacting technique for evaluation of stresses in engineering components, e.g [3]. An infrared detector is used to measure the small temperature change associated with the thermoelastic effect. The output from the detector is termed the 'thermoelastic signal', S, and for orthotropic materials, such as composites, is related to the changes in the sum of the stresses in the principal material directions on the surface of the material, $\Delta\sigma_1$ and $\Delta\sigma_2$, as follows [4]:

$$(\alpha_1\Delta\sigma_1 + \alpha_2\Delta\sigma_2) = A^*S \qquad (1)$$

where α_1 and α_2 are coefficients of linear thermal expansion in the principal material directions and A^* is a calibration constant.

The application of TSA for quantitative stress/damage analysis of composite materials is not straightforward. The first complication is that as damage evolves the specimen heats leading to localised temperature changes at the damage site. This affects the thermoelastic signal and a means for correcting this temperature increase has been devised [5]. Further to this, as the damage evolves the elastic properties of the material change and therefore the stress in the surface ply will change for the same given load. A means of interpreting and calibrating the thermoelastic signal in terms of strain has been devised [6]. Therefore TSA can provide valuable real-time information on the resultant integrity of the component by analysing the stresses/strains at the damage site.

For the current feasibility study qualitative analysis of three sandwich beams has been completed; 1. undamaged, 2. moderate damage and 3. severe damage. The aim of this work was to investigate the possibility of using the thermoelastic signal in a damage assessment, despite the inhomogeneous response provided by the woven structure of the composite. To use TSA specimens must be under a cyclic load. For an initial investigation the beams were loaded in tension at an amplitude of 0.3 mm around an offset of 3.5 kN, at a frequency of 10 Hz to demonstrate the effect of the weave on the response. The results are shown in Figure 9. The weave pattern is clear and regular and the response is such that good noise free readings can be obtained.

Two beams were loaded in the four-point bending rig (see Figure 8(b)) under an increasing quasi-static load until damage initiated. Another beam is tested at a higher load that produced a larger portion of damage. Each of the three beams were reloaded into the rig and loaded at an amplitude of 1.5 mm around an offset of 2 mm at a frequency of 7.5 Hz to obtain the TSA data. The results can be seen in Figure 10. The topmost image represents the undamaged specimen, the centre the moderately damaged and finally the bottom image is the severely damaged specimen.

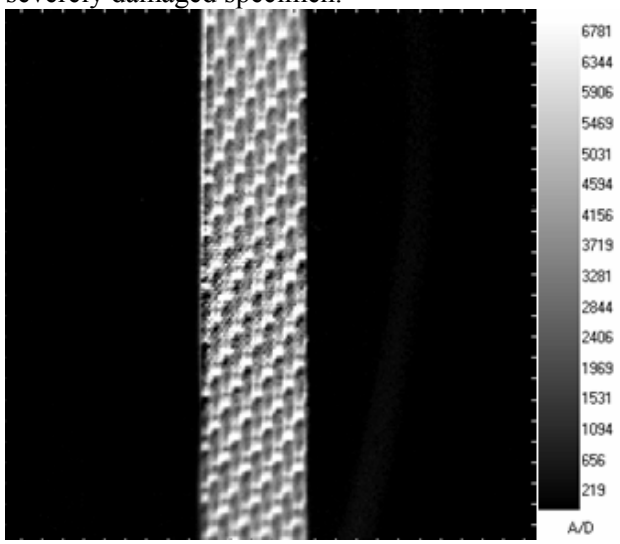

Fig 9. Weave pattern from TSA in tension

The thermoelastic signal plotted in Figure 9 shows the stresses in the different parts of the woven composite. The five harness satin weave used for this specimen has a diagonal pattern of longitudinal and transverse fibre bundles. In Figure 9 diagonal lines of light and dark are evident and can be interpreted as lines of differing stress. Higher stress in the longitudinal fibre bundles to that in the transverse fibre bundles.

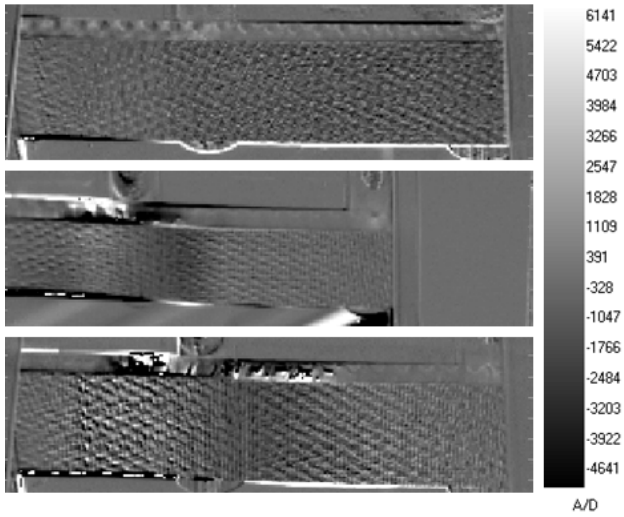

Fig 10. TSA image data

It is immediately obvious that the undamaged specimen demonstrates an even signal across the length of the constant stress section of the beam, besides the pattern from the weave. However, both the moderately and severely damaged specimens show a lighter region around the subsurface damage. This indicates a change in the stress state in this area of the surface skin. From closer inspection of the signal along a line plot on the centre of the surface, it is possible to infer how the stress state changes.

Figure 11 shows a line plot through the data from the undamaged specimen. The raw signal in blue shows the variation caused by the weave pattern n the surface. However, taking a moving average of the data (period 9) it becomes clear that the signal is constant along this region, as expected in the constant stress area.

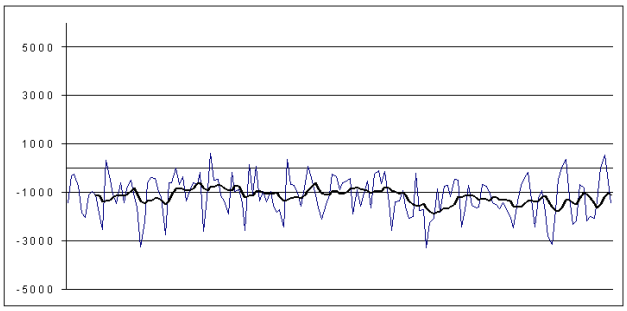

Fig 11. Undamaged specimen

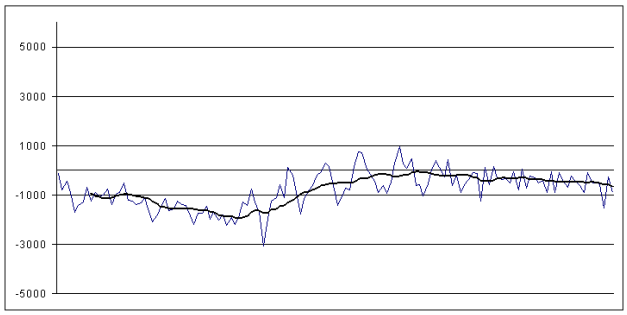

Fig 12. Moderate damage

Figure 12 is a line plot of the moderately damaged specimen. The black, moving average, plot illustrates a reduction in signal around the damaged region, but also a corresponding rise in the signal around the damaged site. The carbon fibre skin in the damaged area is no longer correctly bonded to the core and therefore the stress transfer has been altered. The skin on either side of the damaged site shows an increased stress as this must compensate for the detached skin in the damaged area.

Finally, Figure 13 is a line plot of the severely damaged specimen. A similar trend to the moderately damaged specimen can be seen. The concept of using TSA to monitor a structure with a weave pattern with mirrors has been proven when the structure is under loads that require strength from the skin, core and skin/core bond. However, maintaining the cycle frequency required for TSA with the pressure rig is not proven as yet. Work is still required to calibrate the data to yield quantitative results.

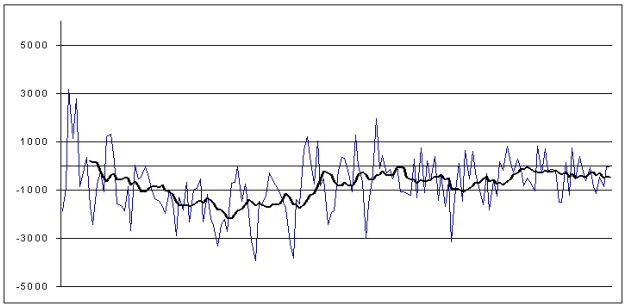

Fig 13. Severe damage

5.2 Pulsed Phase Thermography (PPT)

Pulsed Phase Thermography (PPT) is a relatively new approach that combines the traditional infrared thermography techniques of pulse and modulated thermography [7]. The main advantage of the PPT approach is its portability. The technique subjects the structure under evaluation to a pulse of heat energy that propagates through the structure. In this study the technique is being used in reflection mode, and as such a sequence of infrared images is collected from the same surface the initial pulse was directed at. The images capture the thermal energy that has been reflected off the structure. Mathematically the thermal pulse can be decomposed into a multitude of individual sinusoidal components [7] as such various amplitudes and frequencies are reflected from different levels of the structure from the single pulse. The frequency content of these sinusoidal components, that are reflected from the structure and appear on the surface, can be obtained from the thermal images recorded through a Fourier transformation analysis. The basis for PPT is the comparison of various specified frequency ranges, using a discrete one-dimensional Fourier transform at each pixel in the image. The output is provided in terms of the amplitude and phase of the frequency wave at the surface. The output is referenced relative to each pixel, at time t, in the field of view and as such no reference input is required. Assuming any deviation in the phase or amplitude

results is a consequence of the specific reflection path. The reflection from the structure is influenced by the thermal conductivity, which will be modified at damage sites. Hence the signal will have a different phase to that of the undamaged material, revealing the damage in a phase plot.

For a feasibility test of this technique a pre-damaged sandwich beam was loaded such that the damaged region of the core was detached from the skin offering the highest difference in thermal conductivity and therefore the highest chance of a positive result. To apply the PPT a metered thermal pulse was applied to the sandwich beam using a Cullman camera flash. The thermal images were recorded using a Cedip Silver 450M infrared system positioned 0.5 m from the front surface of the beam.

Figure 14 shows the results from applying PPT to a damaged carbon fibre sandwich beam. The damaged region (circled in red) should be obvious from a change in the phase plot. However it is clear that PPT is not offering the expected results and it can be concluded that if a known region of damage cannot be identified with this technique it will be of little interest as an approach for future testing.

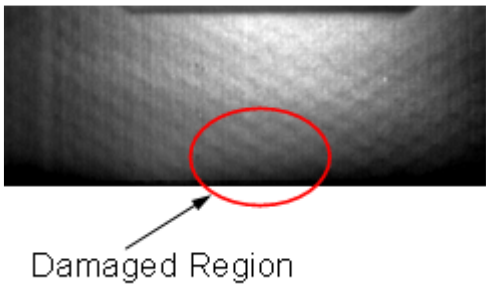

Fig 14. PPT of a damaged sandwich beam

5.3 Digital Image Correlation (DIC)

Another fully non-destructive and non-contact visual technique, Digital Image Correlation (DIC or photogrammetry) is a relatively new and useful tool to map strain distribution across the surface of a deformed component. From the literature it can be shown that the technique has been successfully utilised for heterogeneous engineering materials, such as composites [8-12]. DIC is a visual technique that is used to track surface displacements of deforming materials by recognition of geometrical changes in grey scale distribution on surface patterns before and after straining [8]. All that is required for DIC analysis is an unstrained (reference image) and a strained (deformed image) that can be compared to the reference image [13]. The DIC method is as follows:

1. Apply a regular grid of nodes (e.g. 10 pixels apart) to reference image.
2. For each node, identify a "subimage" of fixed pixel size (e.g. 40 pixels).
3. In the deformed image, compare the subimage to windows of the same size. This is done by calculating the pixel intensity correlation coefficient:

$$r(m,n) = \frac{\Sigma_i \Sigma_j F(i,j) T(i-m, j-n)}{\sqrt{\Sigma_i \Sigma_j \left[F(i,j)\right]^2} \sqrt{\Sigma_i \Sigma_j \left[T(i-m, j-n)\right]^2}} \quad (2)$$

where F and T are the pixel greyscale values in the reference and deformed images, respectively, and r(m,n) is the correlation parameter at location (m,n).

4. Move the window through a defined area of the deformed image and calculate the correlation coefficient for each location.
5. The location within the highest correlation is the location of the node. Subtract the new location from the old to determine the displacement of the node.
6. Repeat steps 2-5 for all nodes of the reference image [9].

Then using a finite element approximation over a 4 noded square element:

$$\varepsilon = Bu \quad (3)$$

where ε is 2D plane strain vector, B contains linear interpolation shape functions and u are the 8 nodal orthogonal nodal displacements.

For this study the feasibility of such a system is to be tested on a simple tensile specimen under a 'pull' test. The specimen is manufactured by MO 2, and as such has a five-harness pattern on the surface of the specimen. The result is skown in Figure 15. the woven structure of the material is not apparent in this plot as the reading is related to the strain which is uniform in the plane.

This feasibility test used a single camera and could therefore only measure in-plane strain. Full-scale testing of pressure loads on the generic panel will use a two camera system that will offer strain measurements in all three axes.

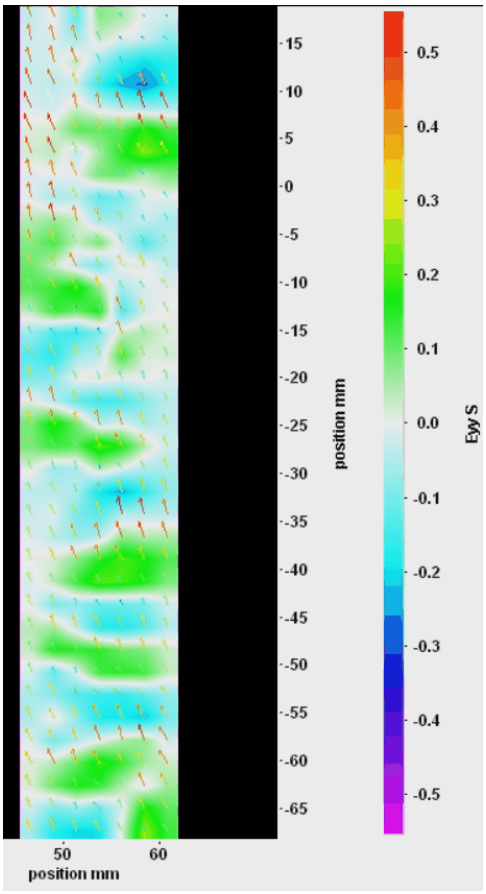

Fig 15. DIC of a carbon fibre tensile specimen

6 Conclusions and Future work

A methodology to use full-scale testing on carbon fibre sandwich secondary structure wing components under a pressure load has been developed such that full-field stress/strain analysis can be performed for comparison with an FEA model. This will be used to make a performance comparison of structure manufactured from different raw material and process combinations (referenced as Manufacturing Options MOs). To simulate the performance of real secondary structure wing components a review was made of such panels previously manufactured at Smiths Aerospace. Three generic component designs were developed incorporating the important features found during the review.

While the pressure test rig is being constructed a feasibility study has been performed on three visual techniques for structural performance monitoring. TSA images on tensile specimens and sandwich beams with varying degrees of sub-surface damage have proved the technique to be capable of both detecting the stress patterns on the surface from a woven component and stress transfer from subsurface damage. PPT has been used to image a sandwich beam with severe sub-surface damage. The image failed to identify the damage and as such would not offer a viable option for the full-scale test. Finally DIC analysis of a tensile woven specimen under a pull-test has shown that it is possible to obtain readings from a single camera system but a two camera system is required to obtain the out of plane displacements.

Future work will use the full-scale pressure test rig to obtain data on panels constructed from the five different manufacturing options to the three different generic designs. A comparison will be made with FEA models using mechanical properties from each of the five manufacturing options. The aim is to investigate the relative performance of the five options and provide a less expensive approach to secondary structure manufacture in the future.

7 References

[1] Gutowski T., Henderson R. and Shipp **C**. "Manufacturing Costs for Advanced Composites Aerospace Parts*"*. *SAMPE Journal*, Vol. 27, pp37-43, 1991.

[2] Qi B., Raju J., Kruckenburg T. and Stanning R. "A Resin Film Infusion Process for Manufacture of Advanced Composite Structures". *Composite Structures*, Vol. 47, pp 471-476, 1999.

[3] Pagan N. and Schoeppner G. "*Comprehensive Composite Materials*". edited by A. Kelly and C. Zweben, Pergamon, Vol 2, 2000.

[4] Pagano N. and Pipes R. *J Comp Mater*, Vol. 5, pp50-57, 1971.

[5] Dulieu-Barton J., Emery T., Quinn S. and Cunningham P. *Meas Sci and Tecnol,* Vol. 17, pp1627-1637, 2006.

[6] Emery T., Dulieu-Barton J., Earl J. and Cunningham P. "A Generalised Approach to the Calibration of Orthotropic materials for Thermoelastic Stress Analysis", in preparation.

[7] Maldague X. and Marinetti S. *J Apply Phys*, Vol. 79, pp2694-2698, 1996.

[8] Godara A. and Raabe D. "Influence of Fibre Orientation on Global Mechanical Behaviour and Mesoscale Strain Localisation in a Short Glass-Fibre-Reinforced Epoxy Polymer Composite During Tensile Deformation Investigated Using Digital Image Correlation", *Compos Sci Technol*, 2007.

[9] Corr D., Accardi M., Graham-Brady L. and Shah S. "Digital Image Correlation Analysis of Interfacial Debonding Properties and Fracture Behaviour in Concrete", *Eng Fract Mechs*, Vol. 74, pp109-121, 2007.

[10] Sachs C., Fabritius H. and Raabe D. "Experimental Investigation of the Elastic-Plastic Deformation of

Mineralised Lobster Cuticle by Digital Image Correlation", *J Struct Biol*, Vol 155, pp409-25, 2006.

[11] Choi S. and Shah S. "Measurement of Deformation on Concrete Subject to Compression Using Image Correlation", *Exp Mech*, Vol 37, pp307-13, 1997.

[12] Lawler J., Keane D. and Shah S. "Measuring Three-Dimensional Damage in Concrete Under Compression", *ACI Mater J*, Vol.98, pp465-75, 2001.

[13] Sutton M., McNeill S., Helm J. and Chao Y. "Advances in Two-Dimensional and Three-Dimensional Computer Vision", *Top Appl Phys*, Vol. 77, pp323-72, 2000.